# Probing the Longitudinal Momentum Spread of the Electron Wave Packet at the Tunnel Exit

A. N. Pfeiffer,[1] C. Cirelli,[1,*] A. S. Landsman,[1,†] M. Smolarski,[1] D. Dimitrovski,[2,‡] L. B. Madsen,[2] and U. Keller[1]

[1]*Physics Department, ETH Zurich, 8093 Zurich, Switzerland*

[2]*Lundbeck Foundation Theoretical Center for Quantum System Research, Department of Physics and Astronomy, Aarhus University, 8000 Aarhus C, Denmark*

(Received 18 November 2011; revised manuscript received 30 January 2012; published 21 August 2012)

We present an ellipticity-resolved study of momentum distributions arising from strong-field ionization of helium. The influence of the ion potential on the departing electron is considered within a semiclassical model consisting of an initial tunneling step and subsequent classical propagation. We find that the momentum distribution can be explained by including the longitudinal momentum spread of the electron at the exit from the tunnel. Our combined experimental and theoretical study provides an estimate of this momentum spread.

DOI: 10.1103/PhysRevLett.109.083002 PACS numbers: 33.20.Xx, 31.15.xg, 32.80.Rm, 33.60.+q

In strong-field physics and attoscience, it is often assumed that tunnel ionization is the first step that initiates the subsequent dynamics [1]. The Coulomb interaction between the liberated electron and the parent ion in the presence of a femtosecond laser pulse is of crucial importance to draw conclusions on various types of time delays in ultrafast experiments [2,3] and also in the case when attosecond pulses are used to promote the electron into the continuum by single photon ionization [4,5]. Semiclassical models are indispensable for guiding ultrafast experiments and devising new schemes for obtaining time resolution. In the semiclassical model of strong-field ionization, the electron first escapes from the atom by tunneling, and then in a second step it follows a classical trajectory, influenced by the parent ion potential and the femtosecond laser pulse. The simplest approach is to neglect the influence of the ion potential on the electron trajectory, the so-called Simpleman model [6–10]. There are, however, several effects that cannot be explained within the Simpleman model. Examples of such effects are Coulomb focusing [11,12], low energy structures at midinfrared laser wavelengths [13,14], and Coulomb asymmetry in above-threshold ionization [15,16]. As the precision of experiments in attoscience increases [2,4], so does the demand for precision in the modeling, and hence more details need to be accounted for by theory [3].

Very recently, a study [3] performed with attosecond angular streaking [17] allowed for the determination of the natural coordinates of the tunneling current flow (tunneling geometry) and showed the importance of accurately accounting for the effective potential [18] in semiclassical models. However, the initial conditions for the evolution of the classical trajectory depend not only on this effective potential but also on the momentum space distribution of the electron at the tunnel exit. The momentum spread of the electronic wave packet in the direction transverse to the field has been studied some time ago [19,20] and also more recently [21,22]. Here we study the longitudinal momentum spread of the electronic wave packet at the tunnel exit point, a quantity that has raised substantial interest and controversy [23,24].

Specifically, we present ion momentum distributions recorded over a continuous scan of the ellipticity. By comparing the experimental momentum distributions with classical trajectory Monte Carlo (CTMC) simulations based on the tunnel ionization in parabolic coordinates with induced dipole and Stark shift (TIPIS) model [3], it is found that the momentum distributions strongly depend on the longitudinal electron momentum at the exit of the tunnel. Using the semiclassical TIPIS model based on CTMC simulations, we provide an estimate of the longitudinal momentum spread of the electron at the tunnel exit. In this sense, our experiment probes the longitudinal momentum spread of the electron at the tunnel exit point.

The experimental setup is explained elsewhere [3]; therefore, the description here is kept brief. A cold target recoil ion momentum spectroscopy [25] setup measures the ion momentum of helium ions, which is the negative of the momentum of the electron measured in coincidence due to momentum conservation. Thus information about the electron momentum distributions can be inferred by measuring the ion momentum distributions. Short laser pulses with a pulse duration of 33 fs (FWHM) at a central wavelength of 788 nm are produced by a titanium:sapphire based laser system. The electric field $\mathbf{F}$ of the pulses is given by (atomic units are used throughout this Letter)

$$\mathbf{F}(t) = \sqrt{I} f(t)\left[\frac{1}{\sqrt{\varepsilon^2+1}}\cos(\omega t + \varphi_{\mathrm{CEO}})\hat{\mathbf{e}}_{\mathbf{x}} + \frac{\varepsilon}{\sqrt{\varepsilon^2+1}}\sin(\omega t + \varphi_{\mathrm{CEO}})\hat{\mathbf{e}}_{\mathbf{y}}\right], \quad (1)$$

where $f(t)$ is the pulse envelope, $I$ is the peak intensity, $\omega$ is the laser frequency, and $\phi_{\mathrm{CEO}}$ is the carrier-envelope-offset (CEO) phase [26]. The parameter $\varepsilon$ designates the ellipticity, the $x$ axis is the major axis of the polarization ellipse, and the $y$ axis is the minor axis of the polarization ellipse. The Keldysh parameter [27] is defined by

 

$$\gamma = \frac{\omega\sqrt{2I_p}}{F_{\max}} = \frac{\omega\sqrt{2I_p(1+\varepsilon^2)}}{\sqrt{I}}, \quad (2)$$

where $F_{\max} = \sqrt{I}/\sqrt{1+\varepsilon^2}$ is the maximum electric field along the major axis of the polarization ellipse and $I_p$ is the ionization potential (24.59 eV for helium). In the experiment we vary the ellipticity at a constant intensity $I$, which is estimated to be 0.8 PW/cm$^2$. Thereby $F_{\max}$ changes, and the Keldysh parameter $\gamma$ varies from $\gamma = 0.51$ for $\varepsilon = 0$ to $\gamma = 0.73$ for $\varepsilon = 1$. We note that in our experimental setup a perfect circularly polarized pulse cannot be produced. The ellipticity is limited to about $\varepsilon = \pm 0.93$, due to the specifications of the quarter-wave plate and the optical spectrum of the laser pulses [28].

Figure 1 shows momentum distributions for various values of the ellipticity obtained with anticlockwise rotating fields (designated by $\varepsilon > 0$). Clockwise turning fields were also employed (designated by $\varepsilon < 0$; see Fig. 2). Considering both helicities reduces systematic errors, because fields with different helicity streak the electron by equal amounts but in opposite directions [3]. The ion momentum distributions emerging after ionization by the short intense laser pulse differ qualitatively for linear ($\varepsilon = 0$) and circular polarization ($|\varepsilon| = 1$). For $\varepsilon = 0$ the distribution in the polarization plane is close to Gaussian with a maximum at zero both along and perpendicular to the field direction; in the case of close-to-circular polarization a torus forms around the center (Fig. 1).

For the case of linear polarization ($\varepsilon \approx 0$) and $|\varepsilon|$ larger than 0.3, the momentum distribution exhibits two lobes; that is, there are two peaks in the radially integrated momentum distribution (angular distribution). For $|\varepsilon| > 0.3$, the position of these peaks is shifted with respect to the minor polarization axis by the offset angle $\Delta\theta$, defined in Fig. 1. This angular shift is absent in the analysis based on

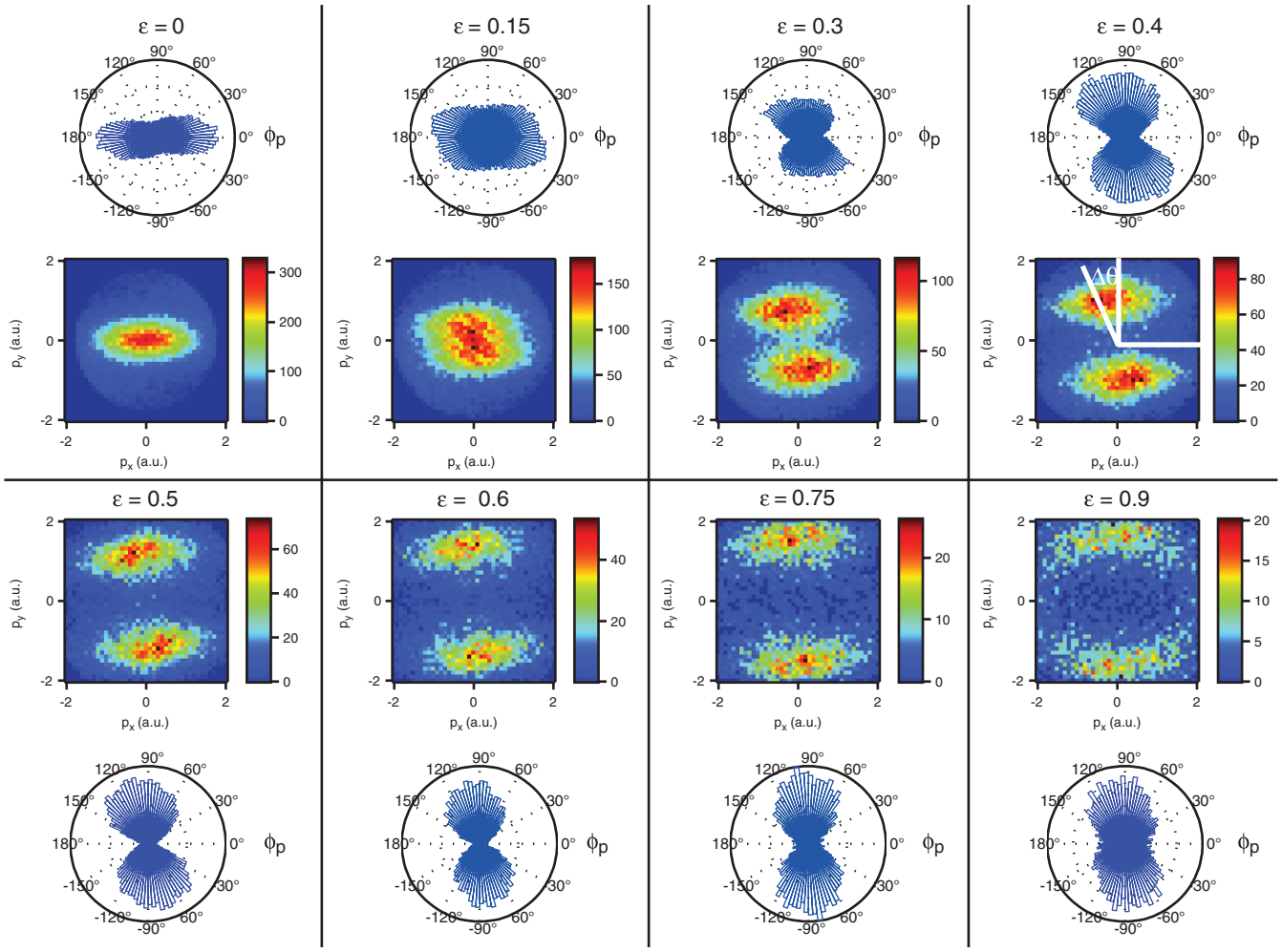


FIG. 1 (color). Ion momentum distributions and angular distributions in the polarization plane for different ellipticities. The major polarization axis is the $x$ axis, the minor polarization axis is the $y$ axis, and $\phi_p = \arctan(p_y/p_x)$ is the angle of the ion momentum $\mathbf{p} = (p_x, p_y)$. For each panel, the presented data (momentum or angular distribution) are integrated over an interval of 0.05 around the ellipticity value indicated in the headline. The offset angle $\Delta\theta$, indicated in the panel for $\varepsilon = 0.4$, is defined as the angle between the peak in the angular distributions and the minor polarization axis of the laser pulse.

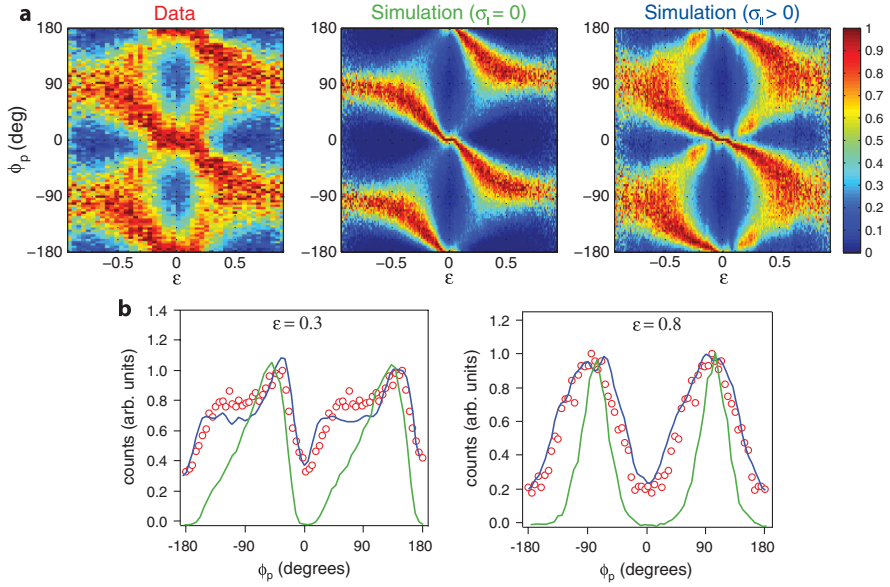


FIG. 2 (color). Ion angular distributions. (a) Ellipticity-resolved angular distributions: the experiment (denoted by "Data"), the simulation with initial longitudinal momentum spread $\sigma_\parallel = 0$, and the simulation with ellipticity-dependent $\sigma_\parallel$ that yields the smallest square error as compared to the experiment (whose values are given in Fig. 3); see the text. The counts of the images are normalized for each fixed value of ellipticity in order to increase visibility. (b) Angular distributions (line cuts through a) for two different ellipticity values. The simulation with $\sigma_\parallel = 0$ (green curve) does not yield four peaks as in the experiment (red markers). The blue curve shows the simulation that yields the least square error; see the text and Fig. 3.

the Simpleman model [10] or using the strong-field approximation [27]. However, it can be accounted for by solving the time-dependent Schrödinger equation and by semiclassical calculation [3]. The offset angle observed in the present experiment, calculated in the tunneling regime [3], is very similar to the Coulomb asymmetry [15,16] of individual above-threshold ionization peaks found in the multiphoton regime. Even though in different dynamical regimes, both effects are manifestations of the influence of the atomic potential. It was shown [3] that the angular shift is very sensitive to the exact form of the parent ion potential of the target atom (see the difference for the angular offset for helium and argon in Ref. [3]) and on the intensity of the laser pulse. Here, another feature can be seen in Fig. 1, and that is the qualitative change in the angular distribution as a function of the ellipticity of the laser pulse. For $|\varepsilon|$ smaller than 0.3, the angular distribution has four peaks, as also predicted recently by calculations based on numerical solution of the time-dependent Schrödinger equation [29]. The four peaks are more clearly visible in Fig. 2, where the angular distributions of electrons integrated over all the energies are shown as a function of ellipticity.

For comparison with the semiclassical model we perform CTMC simulations generating $10^6$ events where the ionization time is distributed according to an empirical ionization rate [30]. The initial conditions, which are the initial electron position $\mathbf{r}_0$ and initial electron momentum $\mathbf{p}_0$, determine the electron trajectory $\mathbf{r}(t)$ obtained by integrating the classical equation of motion

$$\frac{d^2\mathbf{r}(t)}{dt^2} = -\mathbf{F}(t) - \mathrm{grad}[V(\mathbf{r}, t)], \tag{3}$$

where $V$ is the effective atomic potential [18], i.e., $V(\mathbf{r}, t) = -1/r - \alpha\mathbf{F}\cdot\mathbf{r}/r^3$ (for a singly charged parent ion), and $\alpha$ is the ionic polarizability. For helium at the intensity employed in this experiment, the second term in the effective potential is negligible. In all simulations we have assumed a Gaussian envelope $f(t)$ with a FWHM of 33 fs, matching the parameters of the pulse used in the experiment. The initial electron position is the tunnel exit, obtained by using the TIPIS model [3] with the instantaneous value of the electric field at the time of ionization. The initial momentum distribution of the electronic wave packet will be discussed below.

To obtain the angular shift $\Delta\theta$ for ellipticities larger than $|\varepsilon| = 0.3$, it suffices to perform a semiclassical calculation taking, in first approximation, the initial momentum equal to zero. In fact, it suffices to consider only the trajectory corresponding to ionization at the maximum of the field. This can be done, since there is a one-to-one correspondence between the instant of maximum ionization and the maximum in the final momentum distributions, as shown in the supplementary information to Ref. [3].

Below an ellipticity of 0.3, the angular distribution in the polarization plane changes from exhibiting two peaks into having four peaks as shown in Fig. 2(b); see also Refs. [29,31]. In this region of small ellipticity a semiclassical model with no initial electron momentum spread is not able to capture the emergence of four peaks.

Since the initial position of the electron is fixed by the tunnel exit point, we can vary the initial momentum of the electron at birth, thereby varying the initial conditions for Eq. (3), and investigate the influence of that on the final result of the simulations. We note that neither the formation of four peaks in the angular distribution nor the width of the angular distribution can be explained by the recombination of the electron with its parent ion. We have checked within our semiclassical model that the probability for the recombination to happen is less than 1% of the ionization probability [32]; thus, this effect cannot explain our results.

As stated above, in semiclassical models the initial electron momentum is assumed to be zero in a first approximation, but our results suggest that a more detailed description of the electronic wave packet at the tunnel exit is necessary. The initial momentum distribution is usually discussed in terms of its components transversal and longitudinal to the polarization of the electric field. In tunneling theory and not for too strong fields [22], the momentum distribution transverse to the field direction is Gaussian centered at zero and with a standard deviation $\sigma_\perp = \sqrt{\omega/2\gamma}$ [19,20]. This distribution is widely accepted and commonly used in simulations [14,33,34]. An experimental measurement of this distribution using circular light yielded reasonable agreement of data and theory for the wavelength used here [21]. For our parameters $\sigma_\perp$ adapts values ranging from 0.24 a.u. at $\varepsilon = 0$ to 0.20 a.u. at $\varepsilon = 1$ (dashed line in Fig. 3).

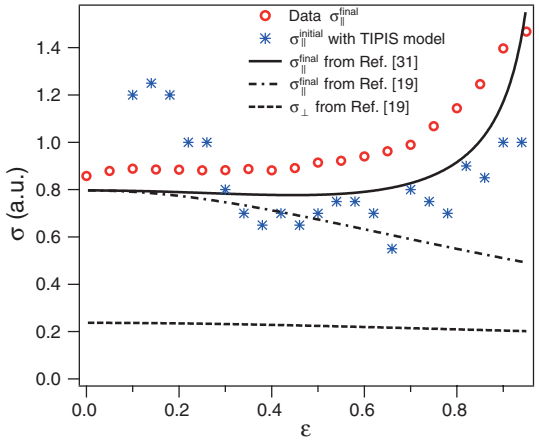


FIG. 3 (color). The blue stars display the value for initial $\sigma_\parallel$, chosen in semiclassical calculations, that yields the least square error with respect to the experimental angular distributions from Fig. 2(b). The red circles are the experimental data for the final momentum spread in the $x$ direction, showing a good agreement with the final longitudinal spread $\sigma_\parallel^{final} = \sqrt{3\omega/2\gamma^3(1-\varepsilon^2)}$ as a function of ellipticity predicted by Ref. [31], depicted as a solid black line. For comparison, the values for the final momentum spread in the perpendicular $\sigma_\perp = \sqrt{\omega/2\gamma}$ (black dashed line) and parallel direction $\sigma_\parallel^{final} = \sqrt{3\omega/2\gamma^3}$ (black dot-dashed line) introduced in Ref. [19] are also shown.

The initial longitudinal momentum distribution at the exit of the tunnel is conceptually more difficult to obtain. The difficulty stems from the fact that the laser field interacts with the ion and the electron during the tunnel ionization process [23]. A formula for the standard deviation of the momentum distribution has been derived only for the final momentum distribution after propagation in the laser field: $\sigma_\parallel^{final} = \sqrt{3\omega/2\gamma^3(1-\varepsilon^2)}$ [31]. The latter is a generalization for any ellipticity value of the standard formula for final momentum distribution in a linearly polarized field, derived by the tunneling theories and introduced in Ref. [19]. Contrary to the final longitudinal spread, the initial longitudinal spread $\sigma_\parallel$ is often assumed to be zero; see, for example, Ref. [14]. Performing semiclassical calculations with this assumption does not reproduce the experimental data (Fig. 2).

We assume that the initial momentum distribution longitudinal to the polarization is Gaussian with a standard deviation $\sigma_\parallel$ and try different values for $\sigma_\parallel$ in the semiclassical simulation. For all ellipticities we find a value for $\sigma_\parallel$ greater than zero that yields a considerably better agreement between data and simulation compared to the assumption of $\sigma_\parallel = 0$. In Fig. 2(b), angular distributions for selected ellipticities are given. For $\varepsilon = 0.8$, the distribution exhibits two peaks, and the positions of the peaks are well reproduced by both assumptions about $\sigma_\parallel$, even though the simulation with $\sigma_\parallel = 0$ greatly underestimates the peaks' angular width. For $\varepsilon = 0.3$, only the simulation with nonzero initial longitudinal spread captures the formation of four peaks in the angular distribution.

The "optimal" value for an initial $\sigma_\parallel$ has been obtained as follows. For any fixed range of ellipticity, CTMC simulations with an initial longitudinal momentum spread ranging from 0 to 1.5 a.u. in steps of 0.05 a.u. are performed, and the one that yields the smallest sum of squared differences with respect to the experimental data is selected.

In Fig. 3, the value of the initial $\sigma_\parallel$ obtained by the semiclassical simulations is displayed together with the experimental values for the final momentum spread. The latter are deduced by a Gaussian fit of the 2D momentum distributions of Fig. 1, projected onto the $x$ axis (major polarization axis). The values given by the various analytical expressions are also given for comparison.

It is interesting to note that for $|\varepsilon| < 0.3$, where the formation of the asymmetric four peaks is the dominant feature in the momentum distribution, the final momentum spread is smaller than the initial spread at the tunnel exit. A possible reason for this is the presence of multiple returns of the liberated electron to the proximity of the ion core. However, the accuracy of the here applied method for finding the initial spread is highest for intermediate values of $|\varepsilon|$ and rather low for the limits $|\varepsilon| = 0$ and $|\varepsilon| = 1$. For values of ellipticity larger than 0.3 the trend is reversed: The optimal momentum spread at the exit of the tunnel is

smaller than the one measured at the detector, the latter being in fairly good agreement (within 10% error) with theoretical predictions.

We have presented measurements of the angular distribution of the ion momenta with a high resolution in ellipticity. Within the semiclassical model, we show that the initial spread of the electron wave packet in the longitudinal direction has a significant impact on the angular distribution of the ion momenta. The good agreement between the experimental data and the semiclassical model provides evidence of the existence and enables access to the momentum spread of the electronic wave packet in the longitudinal direction at the tunnel exit point as a function of ellipticity.

Comparing the initial and the final longitudinal momentum spreads, we observe a crossover between the two quantities when the ellipticity is about 0.3. This is the same critical value where a qualitative change in the momentum distributions happens: The one-to-one correspondence between the time of maximum ionization probability and the peak in the momentum distribution is lost. This raises deeper questions on the validity of classical trajectory approaches near and in the rescattering regime and has implications not only for single ionization but also for the modeling of the experiments on sequential double ionization [35–37].

This work was supported by the NCCR Quantum Photonics (NCCR QP) and NCCR Molecular Ultrafast Science and Technology (NCCR MUST), research instruments of the Swiss National Science Foundation (SNSF), by ETH Research Grant No. ETH-03 09-2 and an SNSF equipment grant, and by the Danish Research Council (Grant No. 10-085430) and an ERC-StG (Project No. 277767-TDMET). A. S. L. is funded by the FP7 IIF (Grant No. 275313).

*cirelli@phys.ethz.ch
†alexandra.landsman@phys.ethz.ch
‡darkod@phys.au.dk

[1] F. Krausz and M. Ivanov, Rev. Mod. Phys. **81**, 163 (2009).
[2] P. Eckle, A. N. Pfeiffer, C. Cirelli, A. Staudte, R. Dörner, H. G. Muller, M. Büttiker, and U. Keller, Science **322**, 1525 (2008).
[3] A. N. Pfeiffer, C. Cirelli, M. Smolarski, D. Dimitrovski, M. Abu-samha, L. B. Madsen, and U. Keller, Nature Phys. **8**, 76 (2012).
[4] M. Schultze *et al.*, Science **328**, 1658 (2010).
[5] K. Klünder *et al.*, Phys. Rev. Lett. **106**, 143002 (2011).
[6] T. F. Gallagher, Phys. Rev. Lett. **61**, 2304 (1988).
[7] H. B. van Linden van den Heuvell, and H. G. Muller, in *Multiphoton Processes*, edited by S. J. Smith and P. L. Knight (Cambridge University Press, Cambridge, England, 1988).
[8] P. B. Corkum, N. H. Burnett, and F. Brunel, Phys. Rev. Lett. **62**, 1259 (1989).
[9] K. C. Kulander, K. J. Schafer, and J. L. Krause, in *Super-Intense Laser-Atom Physics*, edited by B. Piraux, A. L'Huillier, and K. Rzazewski (Plenum, New York, 1993), p. 95.
[10] P. B. Corkum, Phys. Rev. Lett. **71**, 1994 (1993).
[11] T. Brabec, M. Y. Ivanov, and P. B. Corkum, Phys. Rev. A **54**, R2551 (1996).
[12] D. Comtois, D. Zeidler, H. Pépin, J. C. Kieffer, D. M. Villeneuve, and P. B. Corkum, J. Phys. B **38**, 1923 (2005).
[13] C. I. Blaga, F. Catoire, P. Colosimo, G. G. Paulus, H. G. Muller, P. Agostini, and L. F. DiMauro, Nature Phys. **5**, 335 (2009).
[14] C. P. Liu and K. Z. Hatsagortsyan, Phys. Rev. Lett. **105**, 113003 (2010).
[15] M. Bashkansky, P. H. Bucksbaum, and D. W. Schumacher, Phys. Rev. Lett. **60**, 2458 (1988).
[16] S. P. Goreslavski, G. G. Paulus, S. V. Popruzhenko, and N. I. Shvetsov-Shilovski, Phys. Rev. Lett. **93**, 233002 (2004).
[17] P. Eckle, M. Smolarski, P. Schlup, J. Biegert, A. Staudte, M. Schöffler, H. G. Muller, R. Dörner, and U. Keller, Nature Phys. **4**, 565 (2008).
[18] D. Dimitrovski, C. P. J. Martiny, and L. B. Madsen, Phys. Rev. A **82**, 053404 (2010).
[19] N. B. Delone and V. P. Krainov, J. Opt. Soc. Am. B **8**, 1207 (1991).
[20] V. S. Popov, Phys. Usp. **47**, 855 (2004).
[21] L. Arissian, C. Smeenk, F. Turner, C. Trallero, A. V. Sokolov, D. M. Villeneuve, A. Staudte, and P. B. Corkum, Phys. Rev. Lett. **105**, 133002 (2010).
[22] P. A. Batishchev, O. I. Tolstikhin, and T. Morishita, Phys. Rev. A **82**, 023416 (2010).
[23] M. Y. Ivanov, M. Spanner, and O. Smirnova, J. Mod. Opt. **52**, 165 (2005).
[24] A. Czirják, R. Kopold, W. Becker, M. Kleber, and W. P. Schleich, Opt. Commun. **179**, 29 (2000).
[25] R. Dörner, V. Mergel, O. Jagutzki, L. Spielberger, J. Ullrich, R. Moshammer, and H. Schmidt-Böcking, Phys. Rep. **330**, 95 (2000).
[26] H. R. Telle, G. Steinmeyer, A. E. Dunlop, J. Stenger, D. H. Sutter, and U. Keller, Appl. Phys. B **69**, 327 (1999).
[27] L. V. Keldysh, Sov. Phys. JETP **20**, 1307 (1965).
[28] M. Smolarski, P. Eckle, U. Keller, and R. Dörner, Opt. Express **18**, 17 640 (2010).
[29] M. Abu-samha, and L. B. Madsen, Phys. Rev. A **84**, 023411 (2011).
[30] X. M. Tong and C. D. Lin, J. Phys. B **38**, 2593 (2005).
[31] V. D. Mur, S. V. Popruzhenko, and V. S. Popov, J. Exp. Theor. Phys. **92**, 777 (2001).
[32] A. S. Landsman *et al.*, arXiv:1111.6036v1.
[33] W. Quan *et al.*, Phys. Rev. Lett. **103**, 093001 (2009).
[34] T.-M. Yan, S. V. Popruzhenko, M. J. J. Vrakking, and D. Bauer, Phys. Rev. Lett. **105**, 253002 (2010).
[35] A. N. Pfeiffer, C. Cirelli, M. Smolarski, R. Dörner, and U. Keller, Nature Phys. **7**, 428 (2011).
[36] A. Fleischer, H. J. Wörner, L. Arissian, L. R. Liu, M. Meckel, A. Rippert, R. Dörner, D. M. Villeneuve, P. B. Corkum, and A. Staudte, Phys. Rev. Lett. **107**, 113003 (2011).
[37] A. N. Pfeiffer, C. Cirelli, M. Smolarski, X. Wang, J. H. Eberly, R. Dörner, and U. Keller, New J. Phys. **13**, 093008 (2011).